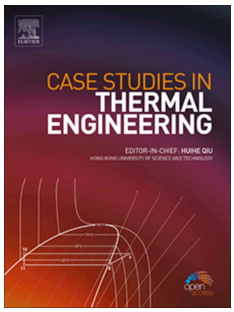
Journal Pre-proof




# Thermal effects of metal implants embedded in different layers of human tissues exposed to electromagnetic fields

Teerapot Wessapan, Phadungsak Rattanadecho

PII: S2214-157X(23)01077-8

DOI: https://doi.org/10.1016/j.csite.2023.103771

Reference: CSITE 103771

To appear in: *Case Studies in Thermal Engineering*

Received Date: 23 July 2023

Revised Date: 16 October 2023

Accepted Date: 13 November 2023

Please cite this article as: T. Wessapan, P. Rattanadecho, Thermal effects of metal implants embedded in different layers of human tissues exposed to electromagnetic fields, *Case Studies in Thermal Engineering* (2023), doi: https://doi.org/10.1016/j.csite.2023.103771.

This is a PDF file of an article that has undergone enhancements after acceptance, such as the addition of a cover page and metadata, and formatting for readability, but it is not yet the definitive version of record. This version will undergo additional copyediting, typesetting and review before it is published in its final form, but we are providing this version to give early visibility of the article. Please note that, during the production process, errors may be discovered which could affect the content, and all legal disclaimers that apply to the journal pertain.

© 2023 Published by Elsevier Ltd.

Journal Pre-proof



# Thermal Effects of Metal Implants Embedded in Different Layers of Human Tissues Exposed to Electromagnetic Fields

Teerapot Wessapan[a] and Phadungsak Rattanadecho[b,*]

[a]Department of Mechanical Engineering, Faculty of Engineering,
Rajamangala University of Technology Thanyaburi, Pathumthani 12110, Thailand.

E-mail: teerapot_w@rmutt.ac.th

[b]Center of Excellence in Electromagnetic Energy Utilization in Engineering (CEEE)
Department of Mechanical Engineering, Faculty of Engineering,
Thammasat University (Rangsit Campus), Pathumthani 12120, Thailand,

E-mail: ratphadu@engr.tu.ac.th*

**Abstract**

Metal implants are typically used in medicine and body modifications to repair or replace damaged tissues, bones, or organs. However, they can cause complications, such as pain, inflammation, and tissue damage, when exposed to strong electromagnetic fields. This study is performed to examine the effect of high-intensity near-field electromagnetic exposure on the thermal effects of metal implants in human tissues. Maxwell's equations and a bioheat model are employed in a numerical simulation to determine the electromagnetic field and temperature distributions in implants and surrounding tissues during exposure to high-intensity electromagnetic fields in close proximity. Various factors are examined, including the implant shape, size, material, and insertion depth. A physical model comprising layers of tissue and metal implants is employed, which is subjected to an alternating electromagnetic field generated by an induction coil. Results show that the implant shape, size, and depth affect tissue heating. Stainless steel 410 implants result in higher tissue temperature increases owing to their greater sensitivity to electromagnetic induction compared with Ti–6Al–4V implants. The findings from this study provide valuable insights into the thermal behavior and electromagnetic interactions of metal implants in human tissues, thus contributing to the advancement of implant design and human safety in electromagnetic environments.

***Keywords: metal implants, thermal effects, electromagnetic fields, human tissues, heat transfer***

Journal Pre-proof


## 1. Introduction

The use of implants in numerous applications has increased significantly in recent years. Metal implants have become widely adopted in the fields of medicine and body modification as they offer effective solutions for repairing or replacing damaged tissues, bones, or organs [1]. Metal implants include joint implants, plates, screws, rods, dental implants, pacemaker leads, brain and cranial implants, stents, cochlear implants, and subdermal implants. They serve various medical purposes such as replacing joints, fixing fractures, supporting cardiac devices, and enhancing body modifications. Figure 1 shows the various applications of metal implants. Titanium, and stainless steel are used frequently in metal implants [2]. However, metal implants can impose adverse effects when subjected to strong electromagnetic fields (EMFs).

EMFs generated by various sources such as television transmitters, and mobile phones can interact with metallic implants in human tissues [3]. Meanwhile, devices such as electromagnetic induction heaters, induction cooktops, transformers, and electromagnetic coils can induce electrical currents in metal objects via electromagnetic induction [4]. Electromagnetic induction can generate an EMF that heats the implant and surrounding tissues. This can result in pain, inflammation, and tissue damage of varying severity levels based on factors such as the EMF magnitude, implant type, and individual sensitivity of the patient [5].

Studies regarding the mechanism by which EMFs generated by diverse sources interact with metallic implants in human tissues are limited by the scarcity of precise and realistic body parts and EMF models [6]. In addition, the direct testing of the effects of electromagnetic waves on patients presents ethical limitations. Thus, determining the effect of EMF exposure on patients with implants is difficult. Researchers have proposed various novel methods to overcome issues associated with interactions between EMFs and metallic implants, including computational modeling [7-8], experiments [9], and cadaveric studies [10]. Previous research has mostly concentrated on the influence of EMFs on implants and currents induced within implants without considering heat transfer [11]. Some studies have focused on the relationship between EMFs generated from diverse sources and metallic implants placed in human tissues [12].

To ensure safety, the International Commission on Non-Ionizing Radiation Protection specifies limitations for EMF exposure in terms of the specific absorption rate but does not define the specific temperature guidelines directly [13]. Even a slight increase in tissue

Journal Pre-proof

temperature caused by the interaction between EMFs and implants is detrimental to health [14]. Moreover, the heating of tissues surrounding implants caused by EMF exposure can impose adverse effects. Individuals may experience tissue damage, inflammation, and discomfort because of these effects [15]. Although the temperature increase may appear insignificant, it may disrupt the normal functioning of tissues [16] and degrade the functionality of the implant [17]. Consequently, even slight temperature increases generated by EMF-induced heating should not be disregarded as they can adversely affect the overall health and well-being of patients with implants. Thus, the hazards associated with EMF exposure must be understood and reduced [18]. Tissue thermal models, including the Pennes bioheat equation [19] and its derivative, the Chen and Holmes model [20], are pivotal in understanding the thermal effects of metal implants. Additionally, a more recent addition to this field is the Porous Media model [21-22]. Previously, we extensively examined the effects of EMFs on human body exposure [23–25]. Recently, we focused on investigating the effects of external metal objects on energy absorption and temperature distribution within the human body [26]. However, their effects on the thermophysiological responses of tissues embedded with various metal shapes in different tissue layers are yet to be elucidated. Moreover, studies regarding the effects of electromagnetic induction in the vicinity of implants within the body is limited. A comprehensive understanding of the thermal and electromagnetic effects that occur in human tissues when metal implants are exposed to high-intensity EMFs is crucial. This study directly extends from our prior research [27] by further investigating the interaction between electromagnetic fields and metals, with a specific focus on the thermal effects of metal implants in human tissues exposed to high-intensity near-field electromagnetic fields.

This study highlights the significance of implant characteristics in determining the extent of tissue heating and the resulting complications. The aim is to examine the effect of high-intensity near-field electromagnetic exposure on the thermal effects of metal implants on human tissues. Mathematical modeling is employed to investigate the thermal effects on the tissue surrounding metal implants while considering various factors such as the implant geometry, size, material, and insertion depth. Mathematical characterization of the EMF is achieved using Maxwell’s equations, which are then coupled with the bioheat model to quantify the heat generation and subsequent transfer processes. A physical model comprising layers of tissue and metal implants subjected to an alternating EMF generated by an induction coil is employed. The accuracy of the numerical model is validated by comparing the temperature values with those reported in relevant studies. The analysis reveals significant

associations between implant characteristics (particularly the implant material, geometry, size, and depth) and tissue heating. The results of this study provide invaluable insights into the intricate thermal behavior and electromagnetic interactions of metal implants in human tissues.

## 2. Problem formulation

When metals are embedded in tissues, high-intensity EMFs can induce significant thermal effects. The interaction between these metals and EMFs can result in the generation of eddy currents, thus resulting in the absorption of electromagnetic energy and the subsequent heating of surrounding tissues. However, the precise characteristics of this induction heating phenomenon, particularly in terms of distributions of skin temperature, are yet to be elucidated. Figure 2 illustrates the induction heating process, in which a scenario involving metals embedded beneath the skin and subjected to high-intensity EMFs is depicted. The heating patterns and temperature changes within the skin tissue caused by the embedded metals require further investigation.

## 3. Methods and model

This study investigates the thermal effects of metal implants embedded in various layers of human tissues when subjected to high-intensity near-field electromagnetic exposure. The numerical simulation model employed in this study comprised a tissue layer and an induction coil. Various geometries of metallic materials embedded in tissues, such as plates, spheres, and pins, were considered to represent different implant scenarios. To assess the effects of EMFs, the induced and spatial distributions of fields generated by the induction coil in the model were first determined, which enables a comprehensive understanding of the EMF behavior within the tissue. Subsequently, the energy absorption process was evaluated to analyze the resulting temperature changes in the metal implants and surrounding tissues. Additionally, other interactions were considered to provide a holistic assessment of the thermal effects.

### 3.1 Physical Model

In this study, a two-dimensional (2D) axisymmetric model was employed to represent the vertical cross-section of a three-dimensional model. The physical model comprised a multilayered tissue model measuring 14 mm wide and 11.575 mm high [27]. The tissue model comprised four types of tissues: epidermis, dermis, subcutaneous fat, and muscle. Each tissue layer featured distinct dielectric and thermal properties, which were determined based on a comprehensive literature review (see Table I) [28-29]. To simplify the analysis, each tissue

Journal Pre-proof

layer was assumed to be homogeneous, electrically isotropic, and thermally isotropic [27]. Chemical reactions and phase changes within the tissues were not considered. Figure 3 shows the physical model used in the numerical simulation. Two main elements were present, i.e., the tissue layer model and induction coil (Fig. 3 a); additionally, metal materials of different shapes (plate, sphere, and pin) wee embedded within the tissues (Fig. 3 b). The metal materials exhibited specific geometries: the plate had a diameter of 5 mm and a thickness of 0.2 mm, the sphere had a diameter of 2 mm, and the pin had a diameter of 0.5 mm and a length of 5 mm. The induction coil was positioned in front of the skin segment, at a fixed distance of 20 mm from the skin surface. When an alternating current is generated, the metal undergoes electromagnetic induction heating. The coil configuration comprised three turns with a diameter of 2 mm, which delivered 5 W of power at a frequency of 100 kHz. This physical model provides a basis for conducting numerical simulations pertaining to the thermal effects of metal implants under the effect of EMFs.

### 3.2 Equations for EMF Analysis

To simplify the problem, certain assumptions were introduced in the mathematical model. These assumptions are associated with the representation of the EMF and its oscillations, along with the resulting physiological processes arising from the interactions between the EMF and materials.

1. The EMF is modeled using a 2D axisymmetric geometry.

2. The interaction between the EMF and metal and tissue occurs within an open space.

3. The free space is truncated using an infinite element domain.

4. The dielectric properties of both the metal and tissue are constant.

Maxwell's equations were employed to elucidate the propagation of EMFs through the medium. These equations mathematically express the interrelated characteristics of electromagnetic phenomena. To illustrate the EMF that permeates the medium during induction heating, we employed simplified Maxwell's equations [30] as follows:

$$\nabla \times \mathbf{H} = \mathbf{J}, \tag{1}$$

$$\mathbf{B} = \nabla \times \mathbf{A}, \tag{2}$$

$$\mathbf{E} = -j\omega\mathbf{A}, \tag{3}$$

$$\mathbf{J} = \sigma \mathbf{E} + j\omega \mathbf{D}, \quad (4)$$

where **H** is the magnetic field intensity (A/m), **B** is the magnetic flux density (T), **E** is the electric field intensity (V/m), **A** is the magnetic vector potential (Wb/m), **D** is the electric displacement or electric flux density (C/m$^2$), **J** is the electric current density (A/m$^2$), $\sigma$ is the electrical conductivity of the material (S/m), $j = \sqrt{-1}$, and $\omega = 2\pi f$ is the angular frequency of the magnetic field (rad/s).

The constitutive relationship between the electric field intensity and the electric displacement can be described in a generalized form as follows:

$$\mathbf{D} = \varepsilon_0 \varepsilon_r \mathbf{E}, \quad (5)$$

where $\varepsilon_0$ is the permittivity of free space ($8.8542 \times 10^{-12}$ F/m) and $\varepsilon_r$ is the relative permittivity (dimensionless).

Similarly, the constitutive relationship between the magnetic field intensity and magnetic flux density can be described in a generalized form as follows:

$$\mathbf{B} = \mu_0 \mu_r \mathbf{H}, \quad (6)$$

where $\mu_0$ is the permeability of free space ($1.257 \times 10^{-6}$ H/m) and $\mu_r$ is the relative permeability (dimensionless).

The current density in the direction of the wires for the inductor is expressed as

$$\mathbf{J_e} = \frac{N(V_{coil}+V_{ind})}{AR_{coil}} \mathbf{e}_{\text{coil}}, \quad (7)$$

where $\mathbf{J_e}$ is the externally generated current density (A/m$^2$), $N$ the number of turns in the coil, $\mathbf{e}_{\text{coil}}$ a vector field representing the direction of the wires, $V_{\text{coil}}$ the total voltage across the coil, and $V_{\text{ind}}$ the voltage induced by the integration of the electric field along the coil.

EMFs propagate naturally in infinite space. To confine the calculations to a specific domain, such as free space, an infinite element was employed to truncate the outer layer. The outer boundary of the calculated domain was regarded as a magnetic insulation boundary condition to effectively suppress reflections.

$$\mathbf{n} \times \mathbf{A} = 0, \quad (8)$$

Journal Pre-proof

where **n** is the normal vector.

### 3.3 Equations for Heat Transfer Analysis

In this study, we examined the heat transfer and the resulting temperature increase in tissues implanted with metals when exposed to electromagnetic near fields. The combined effects of the EMF and transient heat transfer were addressed by solving the associated equations. The temperature increase observed in the tissue was due to the absorption of electromagnetic energy by the metal, which was subsequently transferred to the surrounding tissue. To simplify the problem, we introduced the following assumptions:

1. The heat transport is modeled using a 2D axisymmetric geometry.

2. The thermal properties of the tissue and metal are constant.

3. No material phase changes occur during the exposure.

4. No chemical reaction or response occurs within the tissue.

5. The tissue is homogeneous and exhibits thermal isotropy.

Heat transfer through the implanted metal was modeled as heat conduction in a homogeneous medium. The transient conduction heat equation expressed in Eq. (9) was used to model heat transfer within the metal [27].

$$\rho C \frac{\partial T}{\partial t} = \nabla \cdot (k\nabla T) + Q_e, \quad (9)$$

In the heat equation, the electromagnetic heat source, denoted by $Q_e$ (W/m$^3$), encompasses both resistive and magnetic losses [30].

$$Q_e = Q_{rh} + Q_{ml}, \quad (10)$$

where the resistive loss ($Q_{rh}$) is expressed as

$$Q_{rh} = \frac{1}{2}\mathrm{Re}(\mathbf{J} \cdot \mathbf{E}), \quad (11)$$

and the magnetic loss ($Q_{ml}$) is expressed as

$$Q_{ml} = \frac{1}{2}\mathrm{Re}(i\omega\mathbf{B} \cdot \mathbf{H}). \quad (12)$$

Here, Re is the real part of imaginary number, and $i$ is the imaginary unit

In the tissue model, the skin tissue is regarded as a biomaterial with circulating blood. To determine the temperature increase in the skin tissue, Pennes' bioheat equation [19] was solved. The transient bioheat equation effectively captures the thermal energy exchange mechanisms within the tissue and can be expressed as follows:

$$\rho C \frac{\partial T}{\partial t} = \nabla \cdot (k \nabla T) + \rho_b C_b \omega_b (T_b - T) + Q_{met} + Q_e, \quad (13)$$

where $\rho$ is the tissue density (kg/m$^3$), $C$ the heat capacity of the tissue (J/kg·K), $k$ the thermal conductivity of the tissue (W/m·K), $T$ the tissue temperature (°C), $T_b$ the temperature of blood (°C), $\rho_b$ the density of blood (kg/m$^3$), $C_b$ the heat capacity of blood (J/kg· K), $\omega_b$ the blood perfusion rate (1/s), $Q_{met}$ the metabolic heat source (W/m$^3$), and $Q_e$ the external heat source (the electromagnetic heat source) (W/m$^3$). The blood perfusion term $\rho_b C_b \omega_b (T_b - T)$ approximates the heat conduction between the tissue and blood flow in this analysis.

The skin surface, as illustrated in Fig. 3, was regarded as a convective boundary. A convection heat transfer coefficient of 7 W/m$^2$·K was assumed between the skin and air. In addition, the cooling effect of sweat evaporation from the skin surface was quantified as 10 W/m$^2$. The ambient temperature was set at 25 °C [28]. Disregarding heat loss through radiation, the boundary condition can be expressed as follows:

$$-n \cdot (-k \nabla T) = h_{am}(T - T_{am}) + E_{vap}, \quad (14)$$

where $T_{am}$ is the ambient temperature (°C), $h_{am}$ the ambient convection coefficient (W/m$^2$. K) and $E_{vap}$ the heat loss caused by sweat evaporation.

In this scenario, no contact resistance was assumed between the internal tissue layers. Consequently, the internal boundaries were assumed to be continuous.

$$n \cdot (k_u \nabla T_u - k_d \nabla T_d) = 0, \quad (15)$$

$$T_u = T_d, \quad (16)$$

Initially, the temperature distribution within the tissue was assumed to be uniform at the body core temperature of 37 °C. Consequently, a temperature boundary condition of 37 °C was imposed on the deep tissue surface, where the tissue model was truncated. This ensured that the starting temperature within the tissue was consistent with the core temperature of the body.

Journal Pre-proof

### 3.4 Calculation Procedure

The finite element method was employed to solve the governing equations, initial conditions, and boundary conditions. The numerical problem was addressed using an adaptive mesh refinement approach to optimize the computational process. Tissue models implanted with metal and exposed to an EMF were investigated using COMSOL™ Multiphysics. Mesh convergence analysis was performed to determine the ideal number of elements required. Based on the analysis, a grid comprising approximately 10,000 elements was considered suitable. Beyond this element quantity, the accuracy of the simulation results was unaffected. The time step was dynamically determined by the solver using an adaptive algorithm to ensure both the accuracy and efficiency of the simulation results.

## 4. Results and discussion

An EMF was generated using an induction coil (inductor) powered by an alternating current at a frequency of 100 kHz. The magnetic field, electric field, and temperature distributions within the tissue and metal implants during electromagnetic exposure were calculated via numerical simulations using Maxwell's equations and Pennes' bioheat equation. An exposure setting exceeding the skin-damaging temperature threshold of 43 °C was selected [3, 4]. The effects of the implant shape, size, material, and insertion depth were investigated through numerical simulations to determine the effect of electromagnetic induction on the temperature increase of the surrounding tissues. As presented in Section 4.1, the validation test confirms the accuracy of our numerical model.

### 4.1 Model Verification

To validate the numerical model, the temperature values obtained in the present study and those obtained by Ng et al. [28] were compared based on the same geometric model. In the validation, the skin temperature in a three-layer skin tissue model in contact with a heated metal plate was emphasized. For this validation test, the temperature of the heating plate was set to 90 °C. Figure 4 presents the results of the validation test, which show strong agreement between the steady-state temperatures obtained from the current model and those obtained by Ng et al. The graph reveals that the highest temperature was observed on the skin surface closest to the heated metal plate, and as the depth within the skin layers increased, the temperature gradually decreased. This favorable comparison provides substantial confidence toward the accuracy of the current numerical model, particularly in its ability to accurately represent the complex

Journal Pre-proof


processes that occur during the interaction between the human skin and a metal object heated through electromagnetic induction from an external source. The validation results confirm the reliability of the model and enhance its credibility for further analysis and investigation.

### 4.2 Effect of Insertion Depth

Figure 5 illustrates the magnetic flux density distribution within the tissue model exposed to the EMF generated by the induction coil. The highest magnetic flux density of 5.64e-3 T was observed at the bottom of the skin tissue model around the area exposed to the induction coil. The induction coil was positioned in front of the skin segment, at a fixed distance of 20 mm from the skin surface. The magnetic flux density gradually decreased as the distance from the exposure surface increased. This indicates that the intensity of the magnetic field diminished as it penetrated deeper into the tissue layers. Consequently, in the tissue model, the lowest magnetic flux density was observed at the greatest distance from the skin surface. This information pertaining to the magnetic flux density distribution is useful for analyzing the thermal effects of metal implants embedded in different layers of human tissues when exposed to EMFs.

The effect of implant depth on the temperature distribution of tissues was investigated in this study to analyze the thermal effects of metal implants embedded in various layers of human tissues when exposed to electromagnetic near fields through electromagnetic induction heating. The metal plate used as the metal object had a diameter of 5 mm and a thickness of 0.2 mm. Figure 6 shows a visual representation of the temperature distribution within the tissue surrounding the metal plate at different insertion depths. When the metal plate was in contact with the outer skin (see Fig. 6a), the maximum temperature recorded on the skin surface was 38.52 °C, which indicates that the plate was in direct contact with the outermost layer of the skin. As the insertion depth increased, the maximum temperature observed within the dermis was 37.80 °C when the metal plate was embedded in the dermis layer (see Fig. 6b). This indicates a decrease in temperature compared with the scenario in which the plate was in contact with the outer skin. When the metal plate was embedded deeper into the issue, i.e., in the skin's fat layer, the maximum temperature recorded in the fat layer was 37.75 °C (see Fig. 6c). Hence, the temperature decreased as the insertion depth increased. Fig. 6d shows that when the metal plate was embedded in the muscle layer, the maximum temperature recorded in the muscle was 37.11 °C. This was the largest insertion depth considered in this study, which exhibited the lowest temperature among all the scenarios. The numerical results presented in

Fig. 6 clearly illustrate that as the insertion depth increased, the maximum temperature within the tissue decreased gradually. This trend can be attributed to the relationship between the insertion depth and the magnetic flux density generated from the induction coil, as shown in Fig. 5, where the magnetic flux density in the tissue decreased with the distance from the surface. Therefore, as the metal was placed deeper into the tissue, the level of electromagnetic induction decreased. Consequently, the heat generated within the metal decreased, thus resulting in lower temperatures exhibited by the surrounding tissues.

### 4.3 Effect of Implant Material

The type of implant material significantly affects the thermal effects of electromagnetic induction, particularly in medical implants. In this study, the tissue thermal effects caused by metal electromagnetic induction were investigated by comparing two typically used implant materials: stainless steel 410 and Ti–6Al–4V. Stainless steel 410 is known for its resistance to staining and its ability to withstand harsh environments, thus rendering it suitable for various medical implants, such as orthopedic and dental components. Meanwhile, Ti–6Al–4V is recognized for its biocompatibility, high strength-to-weight ratio, and excellent corrosion resistance, thus rendering it ideal for orthopedic and dental implants. In this study, the thermal effects in tissues with implants fabricated using stainless steel 410 and Ti–6Al–4V were analyzed by considering the coupled effects of electromagnetic near-field distribution and unsteady bioheat transfer, as well as the effects of initial and boundary conditions.

The disparity in tissue temperature between stainless steel and titanium implants can be attributed to their differing responses to induction heating, as described in Table I. Figure 7 shows a comparison of the maximum increase in tissue temperature resulting from the implantation of stainless steel and titanium plates at various depths within the tissue layer at a steady-state temperature. The findings show that the stainless steel implants induced a greater increase in tissue temperature than the titanium implants at all insertion depths. This disparity in the tissue temperature increase can be attributed to the differential sensitivities of the two materials to heat generated via electromagnetic induction. Stainless steel 410 is a martensitic stainless steel containing high amounts of iron and carbon, which renders it more responsive to induction heating. In this study, stainless steel 410 exhibited higher hysteresis losses when exposed to alternating magnetic fields, owing to its higher relative permeability (Table I). By contrast, Ti–6Al–4V exhibited lower hysteresis losses owing to its lower relative permeability (Table I). Consequently, the higher hysteresis losses exhibited by stainless steel 410 due to its

greater sensitivity to alternating magnetic fields resulted in more heat generated during electromagnetic induction. Hence, the temperature increase of the tissues surrounding the stainless-steel implants was higher than that surrounding the titanium implants.

### 4.4 Effect of Implant Geometry

The effect of the implant geometry on the tissue thermal effects caused by electromagnetic induction was investigated. Figure 8 shows a comparison of the temperature distribution in the tissue surrounding metal implants with different geometries under steady-state conditions. The different geometries include a plate (Fig. 8a), sphere (Fig. 8b), and pin (Fig. 8c). The implants were fabricated using Ti–6Al–4V. The plate had a diameter of 5 mm and a thickness of 0.2 mm, the sphere had a diameter of 2 mm, and the pin had a diameter of 0.5 mm and a length of 5 mm. The centers of all the implants were set at the same depth within the tissue.

Based on the temperature distributions, the plate-shaped implant resulted in the highest tissue temperature (Fig. 8a). The larger surface area of the plate-shaped implant parallel to the skin layer facilitated more effective heat generation via induction within the plate. Additionally, the larger surface area allowed for enhanced heat dissipation from the plate to the surrounding tissue. Meanwhile, the parallel orientation of the plate to the induction coil enhanced electromagnetic coupling, thus increasing heat generation within the tissue. By contrast, the pin-shaped implant in the vertical position exhibited the lowest tissue temperature (Fig. 8c). The small diameter of the pin (0.5 mm) limited its surface area for heat transfer. Furthermore, the vertical position of the pin implant relative to the induction coil reduced the electromagnetic coupling, thus resulting in lower heat production within the pin and hence a lower tissue temperature. The sphere-shaped implant exhibited a moderate temperature increase in the surrounding tissue as compared with the plate- and pin-shaped implants (Fig. 8b). The surface area of the sphere (whose diameter was 2 mm) was between those of the plate and pin, which enabled moderate heat generation and dissipation, thus resulting in a moderate temperature increase. Additionally, the rounded shape of the sphere facilitated reasonable electromagnetic energy absorption and heat generation within the object, as well as heat dissipation to the surrounding tissue.

Journal Pre-proof


### 4.5 Effect of Implant Size

The effect of the implant size on the tissue thermal effects caused by electromagnetic induction can be discussed by referring to the values provided in Fig. 9. Figure 9 shows a comparison of the steady-state temperature distribution in the tissue surrounding titanium sphere implants with different diameters: 2 mm (Fig. 9a), 3 mm (Fig. 9b), and 4 mm (Fig. 9c). The spherical implants were fabricated using titanium (Ti–6Al–4V), which is a typically used biocompatible material. In this study, the centers of all spherical implants were set at the same depth, and the variation in implant size was the primary factor contributing to the obtained temperature differences.

The results showed that the size of the spherical implants significantly affected the surrounding tissue temperature. The 2 mm sphere implants showed a maximum temperature of 37.3 °C (Fig. 9a). Increasing the sphere diameter to 3 mm resulted in a higher maximum temperature of 38.21 °C (Fig. 9b). Furthermore, the largest spherical implants with a diameter of 4 mm resulted in the highest maximum temperature of 40.14 °C (Fig. 9c). These results indicate that as the size of the spherical implants increased, the tissue temperature experienced during electromagnetic induction increased. The increased surface area enhanced the coupling of electromagnetic energy and hence heat generation within the metal, as well as the heat dissipated to the surrounding tissue. Notably, the temperature distribution is also affected by factors beyond size, such as the implant composition and depth. The findings revealed that larger sphere implants exhibited higher tissue temperatures than smaller ones. This is primarily attributed to the larger surface area of the larger spherical implants, which enables substantial heat generation and dissipation to the surrounding tissue.

## 5. Conclusions

In this study, a rigorous numerical analysis was conducted to investigate the thermal effects of metal implants on different layers of human tissues when exposed to high-intensity EMFs. The effects of various implant characteristics, including shape, size, material, and insertion depth, on tissue heating were investigated via numerical simulations.

The results of this study provide valuable insights into the complex thermal behaviors and electromagnetic interactions of metal implants within human tissues under near-field electromagnetic induction. A comparison between stainless steel 410 and Ti–6Al–4V implants revealed that the stainless-steel implants resulted in higher tissue temperatures. This discrepancy can be attributed to the different responses of materials to electromagnetic

induction, with stainless steel exhibiting greater sensitivity and generating more heat. Investigations into the implant geometry showed the significant effect of shape on the tissue temperature, where plate-shaped implants resulted in the highest tissue temperatures. Moreover, this study highlighted the effect of implant size, i.e. larger spherical implants resulted in higher tissue temperatures than smaller implants, thus emphasizing the importance of considering implant dimensions in the assessment of thermal side effects. Moreover, as the implant insertion depth increased, the tissue temperature decreased.

The findings of this study are useful for the design and implementation of metal implants for various applications. By considering the thermal behavior and electromagnetic characteristics of implants, designers can optimize implant design to minimize tissue thermal effects and mitigate potential complications. These insights can contribute to the development of improved safety guidelines to ensure user well-being in electromagnetic environments. In future studies, additional implant characteristics and parameters must be investigated to obtain a more comprehensive understanding of thermal behavior and to optimize the design and utilization of metal implants in medical procedures. The results of this study can facilitate the development of more efficient and reliable metal implants, thus benefitting patients. This study conducted simulations under steady-state conditions, which might not fully capture the dynamic changes in tissue temperature during electromagnetic exposure. Incorporating transient analyses could provide a more comprehensive understanding of the thermal response. Moreover, the effect of tissue heterogeneity, which can be significant in real human bodies, was not extensively explored in our study. Future research should consider a more detailed representation of tissue properties.

**Acknowledgments**

This research was supported by the Science, Research, and Innovation Promotion Funding (TSRI) (grant no. FRB660012/0168). This research block grant was supported by the Rajamangala University of Technology Thanyaburi (FRB66E0703B.1), the National Research Council of Thailand (grant number N42A650197), and the Thailand Science Research and Innovation Fundamental Fund (TUFF41/2566).

**Nomenclature**

| | |
|---|---|
| $A$ | magnetic vector potential (Wb/m) |
| $B$ | magnetic flux density (T) |
| $C$ | specific heat capacity (J/(kg K)) |

Journal Pre-proof

Journal Pre-proof


| | | |
|---|---|---|
| $D$ | electric displacement or electric flux density ($C/m^2$) |
| $E$ | electric field intensity (V/m) |
| $e$ | vector field |
| $J$ | electric current density ($A/m^2$) |
| $H$ | magnetic field intensity (A/m) |
| $h$ | convection coefficient ($W/m^2.K$) |
| $J$ | electric current density ($A/m^2$) |
| $i$ | imaginary unit |
| $k$ | thermal conductivity (W/(m K)) |
| $N$ | number of turns in the coil |
| $n$ | normal vector |
| $Q$ | heat source ($W/m^3$) |
| $T$ | temperature (°C) |
| $V$ | electric potential (V) |
| $t$ | time |

**Greek letters**

| | |
|---|---|
| $\mu$ | magnetic permeability (H/m) |
| $\varepsilon$ | permittivity (F/m) |
| $\sigma$ | electric conductivity (S/m) |
| $\omega$ | angular frequency (rad/s) |
| $\rho$ | density ($kg/m^3$) |
| $\omega_b$ | blood perfusion rate (1/s) |

**Subscripts**

| | |
|---|---|
| $b$ | blood |
| $e$ | external |

Journal Pre-proof

Journal Pre-proof


| | | |
|---|---|---|
| *met* | metabolic |
| *ml* | magnetic loss |
| *r* | relative |
| *rh* | resistive loss |
| 0 | free space, initial condition |

**References**

[1] R. Davis, A. Singh, M. J. Jackson, R. T. Coelho, D. Prakash, C. P. Charalambous, W. Ahmed, L. R. Silva, A. A. Lawrence, A comprehensive review on metallic implant biomaterials and their subtractive manufacturing. Int. J. Adv. Manuf. Technol. 120 (2022) 1473–1530.

[2] H. Hermawan, D. Ramdan, J. R. P. Djuansjah, Metals for biomedical applications, in: R.F. Rezai (Eds.), Biomedical Engineering, IntechOpen., 2011, pp. 411–430.

[3] S. Driessen, A. Napp, K. Schmiedchen, T. Kraus, D. Stunder, Electromagnetic interference in cardiac electronic implants caused by novel electrical appliances emitting electromagnetic fields in the intermediate frequency range: a systematic review, Europace, 21(2) (2019) 219–229.

[4] O. Lucia, P. Maussion, E. J. Dede, J. Burdio, Induction heating technology and its applications: Past developments, Current technology, and Future challenges, IEEE Trans. Ind. Electron. 61 (2015) 2509–2520.

[5] I. A. Shah, Y. Cho, H. Yoo, Safety evaluation of medical implants in the human body for a wireless power transfer system in an electric vehicle, IEEE Trans. Electromagn. Compat., 63(3) (2021) 681–690.

[6] H. Virtanen, J. Keshvari, R. Lappalainen, Interaction of radio frequency electromagnetic fields and passive metallic implants--a brief review, Bioelectromagnetics, 27(6) (2006) 431-9.

[7] Z. Psenakova, M. Smondrk, J. Barabas, M. Benova, R. Brociek, A. Wajda, P. Kowol, S. Coco, G.L. Sciuto, Computational Analysis of a Multi-Layered Skin and Cardiac Pacemaker Model Based on Neural Network Approach, Sensors, 22(17) (2022) 6359.

Journal Pre-proof


[8] O. Bottauscio, A. Arduino, M. Chiampi, L. Zilberti, Simplified modeling of implanted medical devices with metallic filamentary closed loops exposed to low or medium frequency magnetic fields, Comput Methods Programs Biomed, 229 (2023) 107316.

[9] S. Hout, J. Y. Chung, Design and characterization of a miniaturized implantable antenna in a seven-layer brain phantom, IEEE Access, 7 (2019) 162062–162069.

[10] D. Crouzier, L. Selek, B. A. Martz, V. Dabouis, R. Arnaud, J. C. Debouzy, Risk assessment of electromagnetic fields exposure with metallic orthopedic implants: a cadaveric study, Orthop Traumatol Surg Res., 98(1) (2012) 90-6.

[11] J. P. Tokaya, C. A. T. van den Berg, P. R. Luijten, A. J. E. Raaijmakers Marmur, Explaining RF induced current patterns on implantable medical devices during MRI using the transfer matrix, Med Phys., 48(1) (2021) 132-141.

[12] K. Bazaka, M. V. Jacob, Implantable devices-issues and challenges, Electronics, 67(3) (2013) 1–34.

[13] International Commission on Non-Ionizing Radiation Protection (ICNIRP), Guidelines for limiting exposure to electromagnetic fields (100 kHz to 300 GHz), Health Phys., 118(5) (2020) 483–524.

[14] B. D. Knapp, K. C. Huang, The effects of temperature on cellular physiology, Annu. Rev. Biophys., 51(1) (2022) 499–526.

[15] R. D. Lovik, J. P. Abraham, E. M. Sparrow, Potential tissue damage from transcutaneous recharge of neuromodulation implants, Int. J. Heat Mass Transf., 52 (2009) 3518–3524.

[16] C. Hu, H. Zuo, Y. Li, Effects of radiofrequency electromagnetic radiation on neurotransmitters in the brain, Front. Public Health., 9 (2021) 691880.

[17] M. Albanna, Effects of electromagnetic field (EMF) on implantable medical devices (IMD), Int. J. Eng. Res. Gen. Sci., 4(1) (2019) 47–57.

[18] J. S. Brink, Thermal effects associated with RF exposures in diagnostic MRI: Overview of existing and emerging concepts of protection, Concepts Magn Reson Part B Magn Reson Eng., 1 (2019) 9618680.

Journal Pre-proof


[23] T. Wessapan, P. Rattanadecho, Flow and heat transfer in biological tissue due to electromagnetic near-field exposure effects, Int. J. Heat Mass Transfer 97 (2016) 174–184.

[24] T. Wessapan, P. Rattanadecho, Temperature induced in human organs due to near-field and far-field electromagnetic exposure effects, Int. J. Heat Mass Transfer 119 (2018) 65–76.

[25] D. Bhargava, N. Leeprechanon, P. Rattanadecho, T. Wessapan, Specific absorption rate and temperature elevation in the human head due to overexposure to mobile phone radiation with different usage patterns, Int. J. Heat Mass Transfer 130 (2019) 1178–1188.

[26] D. Bhargava, P. Rattanadecho, T. Wessapan, The effect of metal objects on the SAR and temperature increase in the human head exposed to dipole antenna (numerical analysis), Case Stud. Therm. Eng. 22 (2020) 100789.

[30] E. Cano-Pleite, M. Fernández-Torrijos, D. Santana, A. Acosta-Iborra, Heat generation depth and temperature distribution in solar receiver tubes subjected to induction. Appl. Therm. Eng. 204 (2022) 117902.

[19] H.H. Pennes, Analysis of tissue and arterial blood temperatures in the resting human forearm, J. Appl. Physiol. 1 (1948) 93–122.

[28] E. Y. K. Ng, H. M. Tan, E. H. Ooi, Prediction and parametric analysis of thermal profiles within heated human skin using the boundary element method. Philos. Transact. A Math. Phys. Eng. Sci. 368(2010), 655–78.

[29] Boyer, H. E., & Gall, T. L. (Eds.). (1985). Metals Handbook. Materials Park, OH: American Society for Metals.

[27] T. Wessapan, P. Rattanadecho, N. Somsuk, M. Yamfang, M. Guptasa and P. Montienthong, Thermal effects of electromagnetic energy on skin in contact with metal: A numerical analysis, Energies 16 (2023) 5925.

[20] M.M. Chen, K.R. Holmes, Microvascular contributions in tissue heat transfer, Ann N Y Acad Sci. 335.1 (1980) 137-150.

[21] E. Kosari, K.Vafai, Synthesis of flow and thermal transport in porous media as applied to biological applications, J. Heat Transf. 143 (2021) 062701.

[22] T. Wessapan, P. Rattanadecho, Flow and Heat Transfer through a Porous Tumor during High-intensity Focused Ultrasound, Int. J. Heat Mass Transfer 216 (2023) 124501.

# Figures

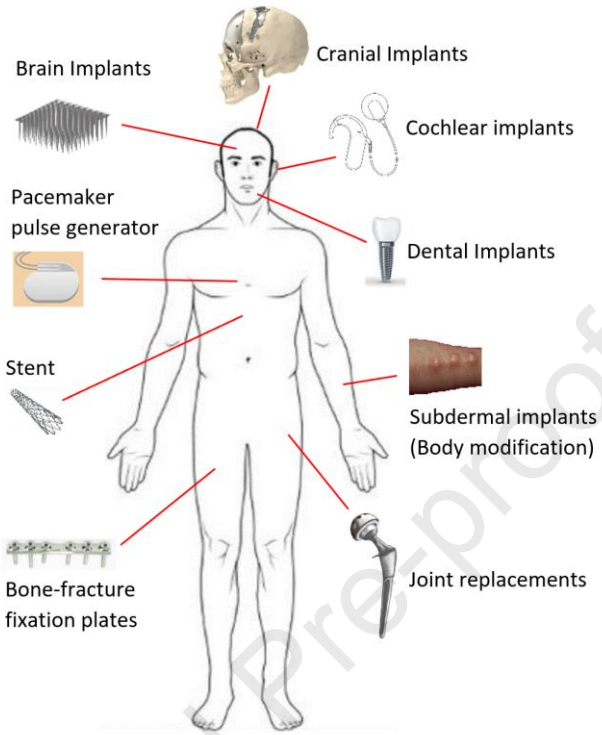



**Fig. 1 Metal implanted in various parts of the human body.**

Journal Pre-proof

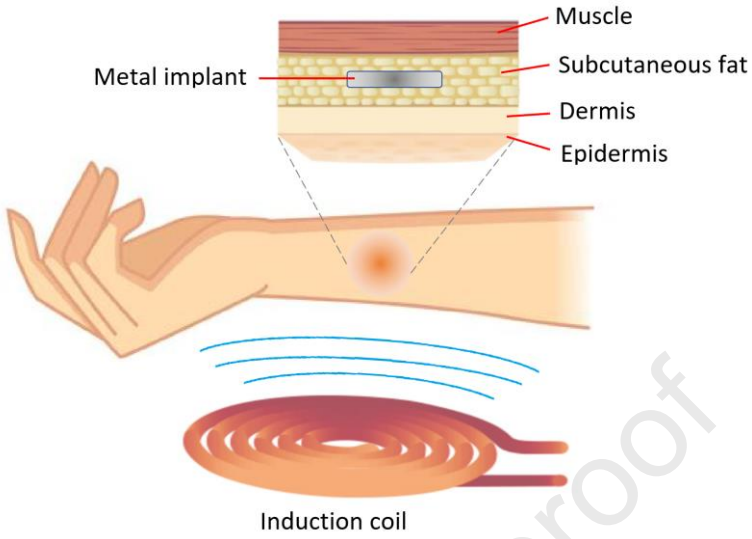
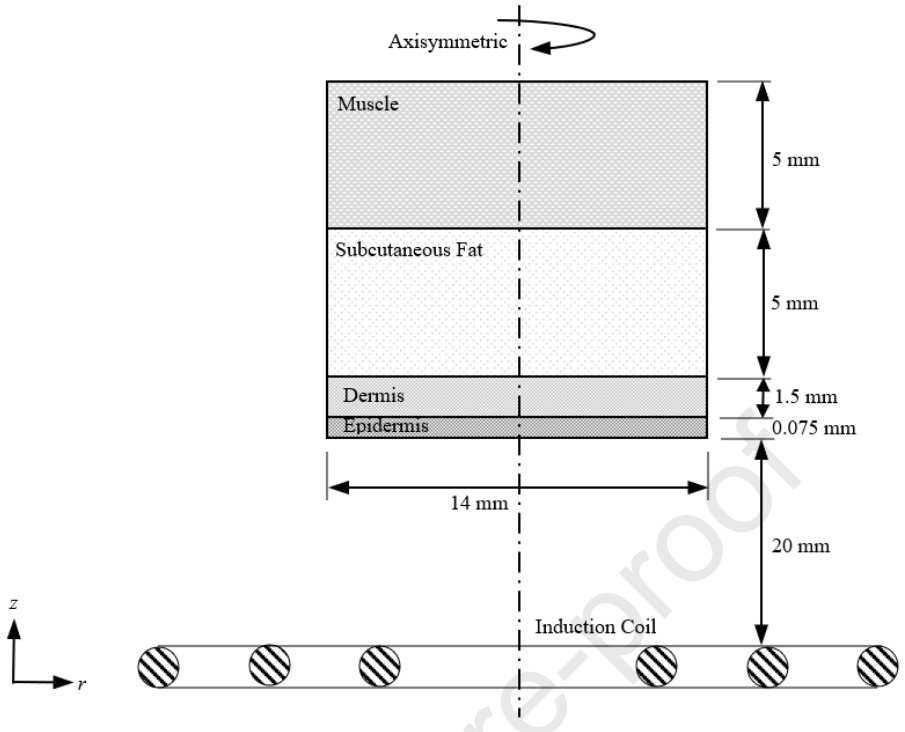
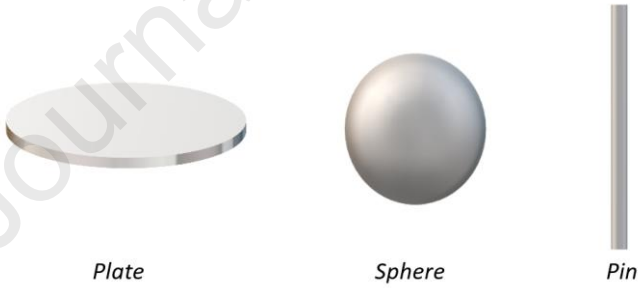



**Fig. 2 Induction heating of metals embedded under the skin from high-intensity electromagnetic fields.**

Journal Pre-proof




(a)




(b)

**Fig. 3 Physical model used in numerical simulation:**
**(a) Tissue layer model and induction coil,**
**(b) Different shapes of metal materials embedded in tissues.**

Journal Pre-proof

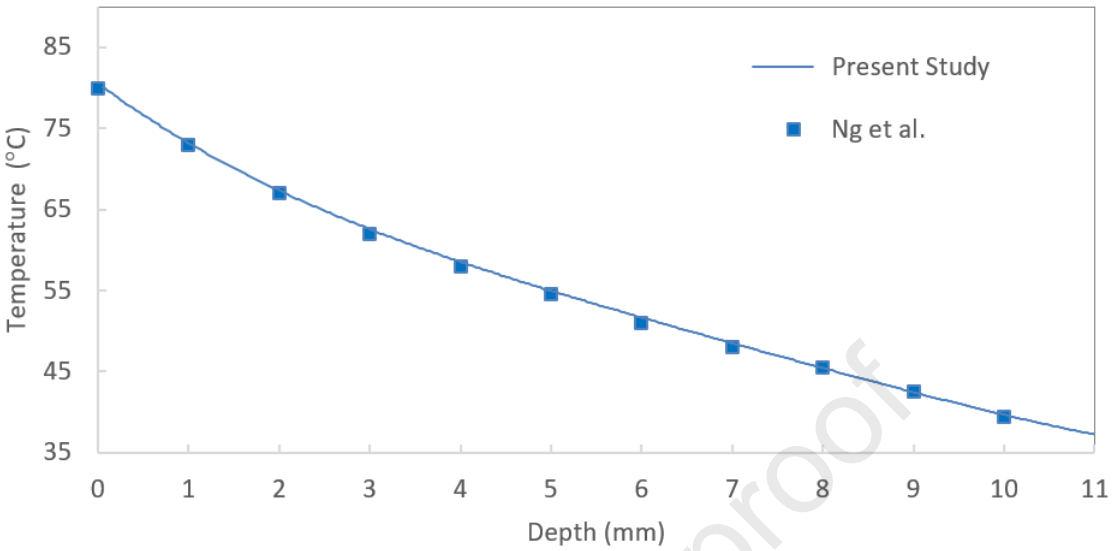



**Fig. 4 Temperature values obtained from mathematical model at various depths compared with those obtained from Ng et al. [28].**

Journal Pre-proof

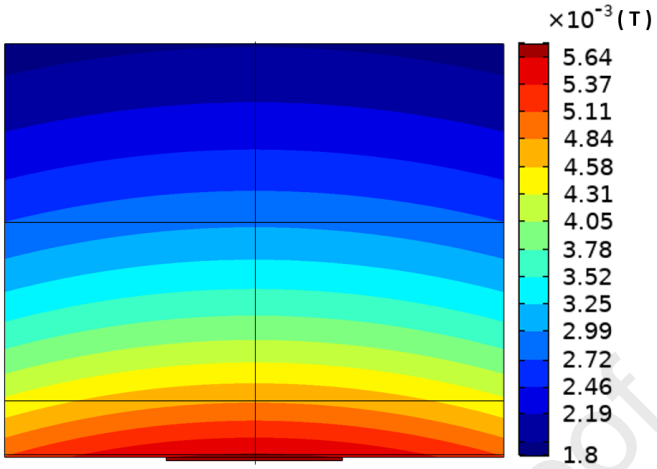



**Fig. 5 Distribution of magnetic flux density in tissue model exposed to electromagnetic field from induction coil.**

Journal Pre-proof

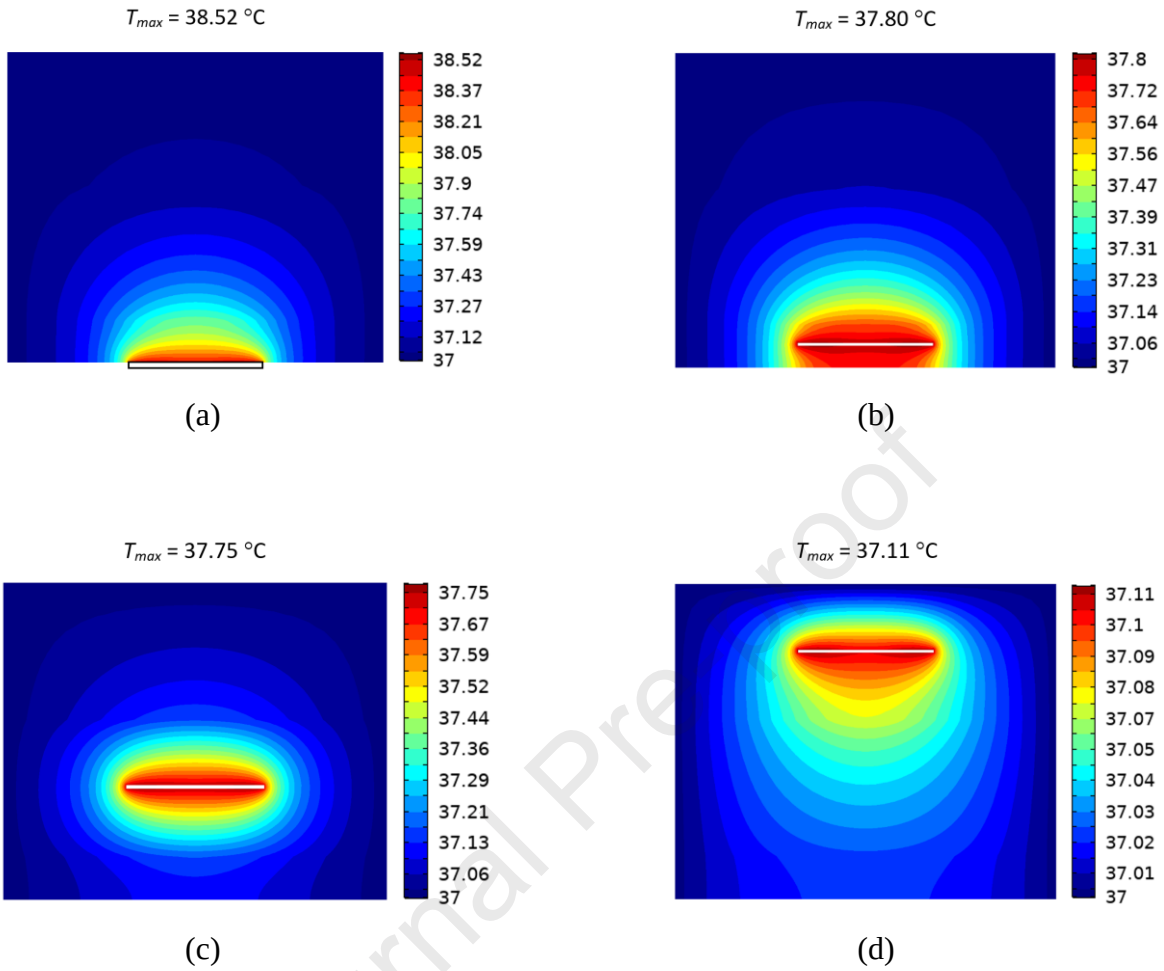



**Fig. 6 Temperature distribution within tissue surrounding metal plate when exposed to electromagnetic waves from induction coil located at the bottom:**
**(a) metal plate is in contact with the outer skin;**
**(b) metal plate is embedded in the dermis;**
**(c) metal plate is embedded in the skin's fat layer;**
**(d) metal plate is embedded in the muscle layer.**

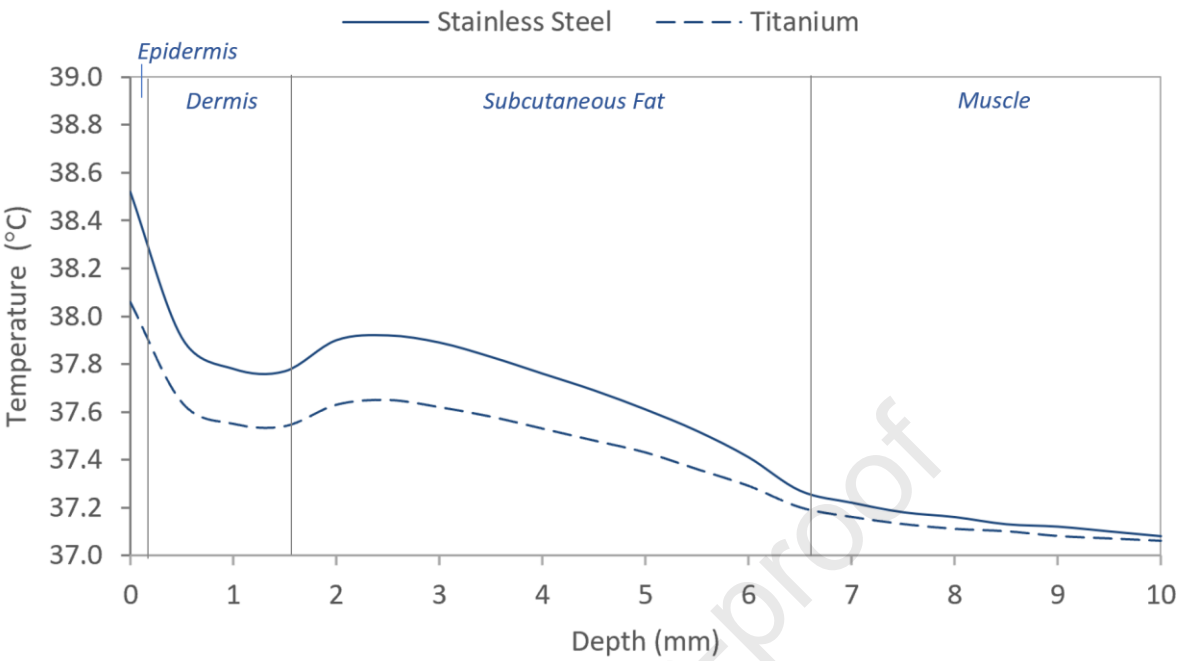
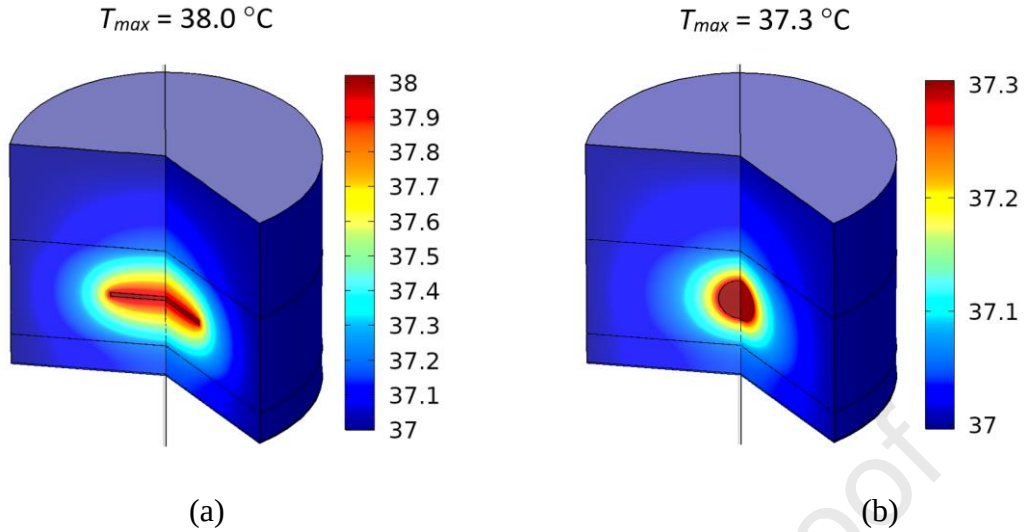
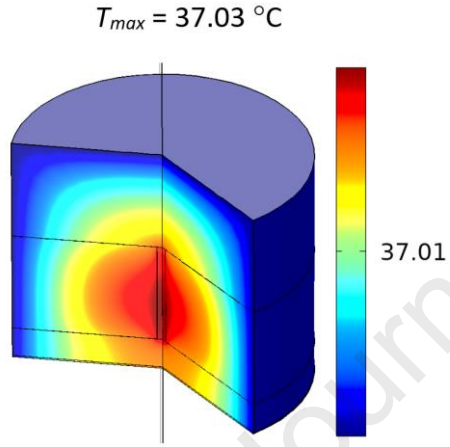



**Fig. 7 Comparison of maximum increase in tissue temperature from implantation of stainless steel and titanium plates in the skin at different depths.**

Journal Pre-proof



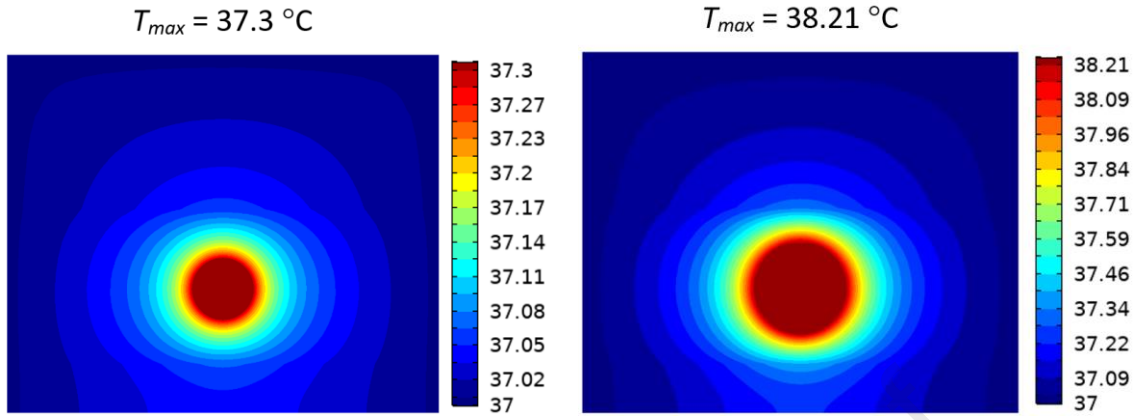

(a) (b)



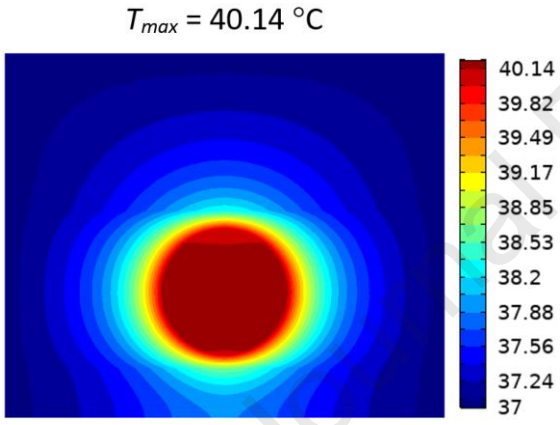

(c)

**Fig. 8 Comparison of temperature distribution in tissue surrounding metal implants based on different geometries: (a) plate, (b) sphere, and (c) pin.**

Journal Pre-proof




(a) (b)




(c)

**Fig. 9 Comparison of temperature distribution in tissue surrounding embedded titanium spheres with different diameters: (a) 2 mm, (b) 3 mm, and (c) 4 mm.**

Journal Pre-proof



# Table

**Table 1. Material properties [28, 29].**

| **Material** | Density ($\rho$) **(kg/m$^3$)** | Thermal conductivity ($k$) **(W/m.K)** | Heat capacity ($C$) **(J/kg°C)** | Blood perfusion rate ($\omega_b$) **(1/s)** | Electrical conductivity ($\sigma$) **(S/m)** | Relative permittivity ($\varepsilon_r$) | Relative permeability ($\mu_r$) |
|---|---|---|---|---|---|---|---|
| Epidermis | 1200 | 0.21 | 3600 | 0.024 | 1.18 | 38.9 | 1 |
| Dermis | 1200 | 0.37 | 3600 | 0.024 | 1.18 | 38.9 | 1 |
| Subcutaneous Fat | 900 | 0.16 | 2500 | 0.00058 | 0.19 | 11.0 | 1 |
| Muscle | 1090 | 0.49 | 3421 | 0.000565 | 0.34 | 53.5 | 1 |
| Air | 1.29 | 0.025 | 1004 | - | 0 | 1 | 1 |
| Titanium Ti-6Al-4V | 4500 | 6.7 | 5263 | - | 5.62e5 | 1 | 1.00005 |
| Stainless Steel 410 | 7880 | 25 | 460 | - | 1.74e6 | 1 | 700 |

Journal Pre-proof

Journal Pre-proof

## Author Statement

**Teerapot Wessapan:** Conceptualization, Methodology, Investigation, Writing – original draft, Funding acquisition.

**Phadungsak Rattanadecho**: Supervision, Funding acquisition.

Journal Pre-proof

Journal Pre-proof

**Manuscript title:** Thermal Effects of Metal Implants Embedded in Different Layers of Human Tissues Exposed to Electromagnetic Fields

**Corresponding author:** Phadungsak Rattanadecho

**Conflicts of interest**
Please declare for each author any conflicts of interest relevant to what you write. This includes employment, consultancies, stock ownership, honoraria, paid expert testimony, patent applications and travel grants. If there are no conflicts of interest, please state that there are none. The information provided here must match the conflicts of interest statement in the manuscript.

**-There are none.**

**Corresponding author declaration**

I certify that there is no conflict of interest relevant to what we write in the manuscript. I certify that the contributors' and conflicts of interest statements included in this paper are correct and have been approved by all co-authors.

Phadungsak Rattanadecho

Oct 16, 2023

Journal Pre-proof